Journal of Superconductivity and Novel Magnetism (2019) 32:1599–1603
https://doi.org/10.1007/s10948-018-4873-7

ORIGINAL PAPER

Phase and Grain Size Dependence of the Pinning Strength of Nanocomposite Magnets

Guosheng Zhang[1] · **Weikang Shan**[1] · **Defeng Guo**[1]

Received: 8 July 2018 / Accepted: 6 September 2018 / Published online: 13 September 2018

Abstract
The pinning of grain interfaces plays an important role in determining the coercivity of nanocomposite magnets. Here, based on pinning effect, a simple model was proposed to correlate the pinning strength with microstructural parameters. A structural factor K has been used to describe the contribution of the phase composition and grain size of hard and soft phases to pinning strength. The model can be used to estimate the pinning strength of nanocomposite magnets, which is important for the design and fabrication of nanocomposite magnets with high coercivity.

Keywords Nanocomposite magnets · Coercivity · Grain interfaces · Pinning strength · Microstructural parameters

1 Introduction

Coercivity, an important magnetic parameter in determining magnetic energy product of permanent magnets, is normally codetermined by the nucleation of reverse domain and the pinning of domain wall [1–7]. These two mechanisms show different dependence on grain size, phase composition, and interface, leading to a complex dependence of coercivity on microstructural parameters. Up to date, several models have been suggested to explain the coercivity variation of a nanocomposite magnet with its microstructural parameters [1, 7–9]. However, most of these models are based on the effect of the exchange coupling on magnetic crystalline anisotropy [7, 9]. The contribution of pinning effect to the coercivity is often underestimated or even neglected.

Many studies demonstrated that the coercivity of nanocomposite magnets with average grain sizes in nanoscale is mainly dominated by pinning mechanism rather than nucleation mechanism due to the existence of numerous grain interfaces [6, 10–13]. This may provide possibilities to correlate the pinning strength with microstructural parameters. Based on the pinning effect, Freideberg and Paul suggested a pinning model to explain how grain interfaces contribute to coercivity in a single-phase permanent magnet [14]. However, such a model is difficult to apply to nanocomposite magnets because of their complicated microstructure.

In this study, a simple model was proposed to describe the relationship between pinning strength and microstructural parameters in a nanocomposite magnet. A popular nanocomposite, $Nd_2Fe_{14}B/\alpha$-Fe, was used as a model material to discuss the dependence of pinning strength on phase composition and grain size. The proposed model describes the dependence of pinning strength on microstructural parameters, which is beneficial for developing nanocomposite magnets with high coercivity.

2 Experimental Details

2.1 Theoretical Model and Formulas

For nanocomposite magnets consisting of soft and hard magnetic materials, reverse domains usually nucleate in the soft-magnetic grains [12, 13]. The reverse domains grow when the reverse magnetic field increases. Given the existence of high-density grain boundaries, the growth of reverse domains is hindered when the domain wall meets a grain interface energy barrier. The pinning strength is a measure of the average magnetic field strength needed to carry the domain wall to pass the intervening energy barrier [14].

✉ Guosheng Zhang
gszhang33@126.com

✉ Defeng Guo
guodf@ysu.edu.cn

[1] State Key Laboratory of Metastable Materials Science and Technology and Key Laboratory for Microstructural Material Physics of Hebei Province, School of Science, Yanshan University, Qinhuangdao 066004, People's Republic of China

A uniform nanocomposite magnet with a grain size smaller than 100 nm is considered in this study. Three types of grain interfaces in the nanocomposite magnet are hard–hard, hard–soft, and soft–soft grain interfaces, which give different pinning barriers because of their different compositions and structures. The total pinning barrier is simultaneously determined by the three kinds of pinning barriers (Fig. 1). To be simple, it is supposed that the pinning strength of each kind of grain interface is constant. The area fractions of the hard–hard, hard–soft, and soft–soft grain interfaces are known as $F_{\rm hh}$, $F_{\rm sh}$, and$F_{\rm ss}$, respectively. Therefore, the pinning strength of the nanocomposite magnet can be expressed as,

$$H_p = F_{hh} \times H_p^{hh} + F_{sh} \times H_p^{sh} + F_{ss} \times H_p^{SS}. \quad (1)$$

where H_p^{hh}, H_p^{sh}, and H_p^{SS} are the pinning strengths of the hard–hard, hard–soft, and soft–soft grain interfaces, respectively.

In the formula (1), the third part related to H_p^{SS} can be neglected because the pinning strength of the soft–soft grain interface is very small [1]. So, the pinning strength of the nanocomposite magnet can be expressed in a simple formula:

$$H_p \approx F_{hh} \times H_p^{hh} + F_{sh} \times H_p^{sh}. \quad (2)$$

The surface area of a grain is proportional to its volume and inversely proportional to its size. For a nanocomposite magnet with a given phase composition and average grain size, it can be simply supposed that the whole surface area of one phase is proportional to its volume fraction and inversely proportional to its average grain size as

$$S_h = k \times \frac{V_h}{d_h}, \quad S_s = k \times \frac{V_s}{d_s}, \quad (3)$$

where S, V, and d denote the surface area, volume fraction, and average grain size, whereas the subscripts h and s denote the hard and soft phases, respectively. To simplify the model, it is supposed that hard and soft grains have a similar grain size distribution, providing a similar coefficient (k) for the two formulas (3). Thus, the surface area fractions of the hard and soft phases can be deduced:

$$f_h = \frac{S_h}{S_h + S_s} = \frac{V_h \times d_s}{V_h \times d_s + V_s \times d_h}, \quad f_s = \frac{S_s}{S_h + S_s} = \frac{V_s \times d_h}{V_h \times d_s + V_s \times d_h}. \quad (4)$$

Furthermore, the grain interface area factions $F_{\rm hh}$ and $F_{\rm sh}$ can be deduced according to the probability theory as

$$F_{hh} = f_h \times f_h, \quad F_{sh} = f_h \times f_s + f_s \times f_h. \quad (5)$$

By combining (4) and (5), the $F_{\rm hh}$, $F_{\rm sh}$, and $F_{\rm ss}$ can be expressed as follows,

$$F_{hh} = \left(\frac{V_h \times d_s}{V_h \times d_s + V_s \times d_h}\right)^2 = \frac{1}{(1+K)^2}, \quad F_{sh} = 2\frac{V_s \times d_h \times V_h \times d_s}{(V_h \times d_s + V_s \times d_h)^2} = \frac{2K}{(1+K)^2}, \quad (6)$$

where K is a structural factor defined as $K = \frac{V_h \times d_s}{V_s \times d_h}$. Therefore, the grain interface area fractions are dependent on the phase composition and relative grain size of two phases.

2.2 Experimental Verification

To examine the validity of our model, $Nd_xFe_{94-x}B_6$ ($x = 8$–10) nanocomposite ribbons with a thickness of 20–30 μm and a width of $\sim$ 2 mm were prepared by melt spinning at a circumferential speed of 14–18 m/s. The microstructure of ribbons was studied by XRD. The average grain sizes and volume fractions of the soft and hard phases in the alloys were determined by analyzing XRD patterns with the Rietveld refinement method [15, 16], in which a crystallographic weighted error of $R_{\rm w} < 10\%$ was obtained. The hysteresis loop of the magnets was measured at room temperature using a vibrating sample magnetometer, yielding the magnetic properties required. The pinning strength of

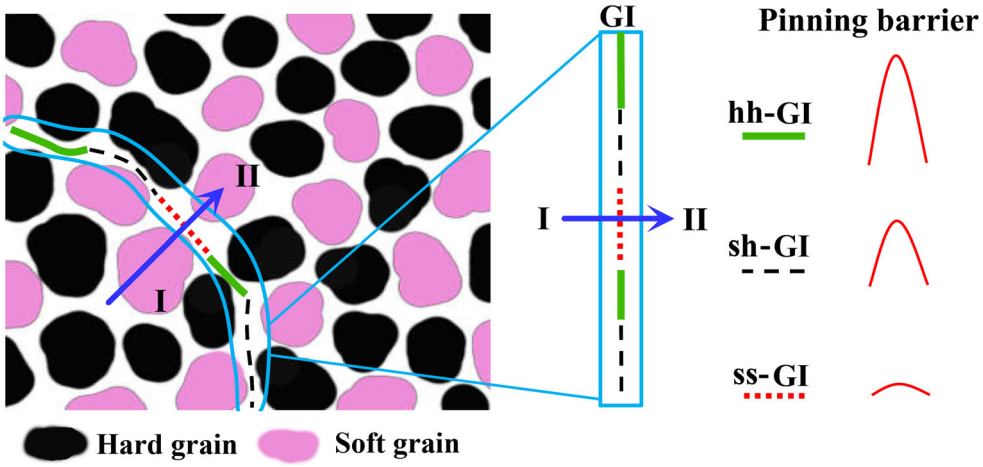

Fig. 1 Schematic diagram of the growth of reverse magnetic domain in a nanocomposite magnet. There are three types of grain interfaces (GIs) in the sample, forming a pinning barrier to hinder the motion of domain wall from regions I to II

Table 1 Microstructure and magnetic parameters of $Nd_xFe_{94-x}B_6$ nanocomposite magnets

Sample		d_s (nm)	d_h (nm)	V_s (%)	V_h (%)	F_{hh} (%)	F_{sh} (%)	H_{ci} (exp)	H_p (exp)	K	$H_{p'}$ (cal)
x	Speed (m/s)										
8	16	18.2	34.6	28.5	70.5	32.0	49.1	4.85	4.45	1.30	4.29
8.5	16	17.3	32.3	24.1	75.9	39.4	46.7	5.30	5.00	1.69	4.78
9	14	24.1	46.8	23.8	76.2	38.7	47.0	5.12	4.47	1.65	4.73
9	16	19.1	34.2	21.1	78.9	45.6	43.9	5.50	5.00	2.09	5.15
9	18	16.7	29.5	22.3	77.7	44.0	44.6	5.90	5.38	1.97	5.06
10	14	24.9	51.2	24.8	75.2	35.5	48.2	5.17	4.40	1.47	4.53
10	15	23.3	43.6	18.7	81.3	48.9	42.1	6.16	5.30	2.32	5.33
10	17	18.8	30.5	15.2	84.8	60.0	34.9	7.10	6.10	3.44	5.93

samples was determined as the field where the irreversible susceptibility of the initial magnetization curve reached the maximum.

3 Results and Discussion

The volume fraction, average grain size of $Nd_2Fe_{14}B$ (hard) and α-Fe (soft) phases, and measured pinning strength of $Nd_xFe_{94-x}B_6$ samples are shown in Table 1. For each sample, the structural factor and grain interface fractions F_{hh} and F_{sh} were calculated by using (6). The grain interface pinning strengths, H_p^{hh} and H_p^{sh}, were determined to be 7.73 and 3.70 kOe by fitting F_{hh}, F_{sh}, and H_p with (2) via the least square method. The fitting resulted in a small standard deviation of $\sim$ 0.23 kOe for the set of data from eight samples (Table 1), thereby demonstrating that the model was reasonable.

A single-phase $Nd_2Fe_{14}B$ with an average grain size of 50–60 nm was prepared via melt spinning at an optimized circumferential speed of $\sim$ 17 m/s. The initial magnetization curve of the sample is shown in Fig. 2, which demonstrated a typical domain wall pinning feature. Its pinning strength was governed by the hard–hard interface because of the absence of the soft phase in the material. A pinning strength of $H_p \sim$ 8.5 kOe was determined by the derivative curve of the initial magnetization curve (inset in Fig. 2). According to the present model, the pinning strength of the sample was calculated to be 7.73 kOe. The calculated value was very close to the experimental value, indicating the reasonability of the model.

Figure 3 presents the dependence of pinning strength and coercivity on the structural factor K. It can be seen that a larger K leads to a higher pinning strength from the calculated H_p–K curve (Fig. 3a). That is, a high-volume fraction and a small grain size for the hard phase, and a low-volume fraction and a big grain size for the soft phase will yield a high pinning strength. Figure 3a also compares the calculated pinning strength with the measured values. The measured pinning strength (solid squares) was similar to the calculated H_p–K curve, thereby demonstrating that the calculated values were reasonable.

Figure 3b presents a comparison of the measured coercivity of the prepared samples (solid stars) and the previously reported Nd–Fe–B alloys prepared via direct melt spinning (hollow triangles and half solid squares) [4, 17]. The same values of $H_p^{hh} = 7.73$ kOe and $H_p^{sh} = 3.70$ kOe were used in the calculation because of similar alloy composition. The measured coercivity increased with the structural factor K, showing the same tendency as the pinning strength. This trend indicates that the pinning mechanism plays a dominant role in determining the coercivity. The half-solid square symbols overlapped with the calculated H_p–K curve, which demonstrated that the pinning mechanism was dominant and the nucleation

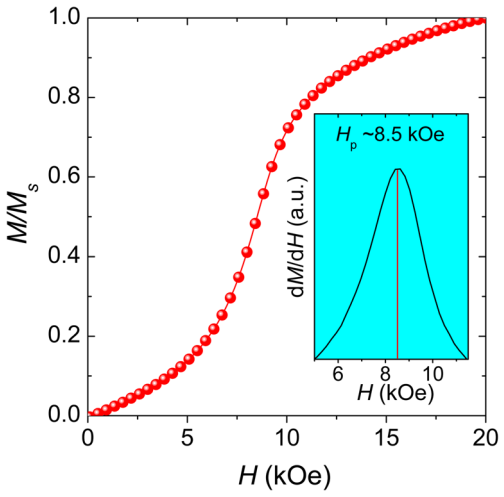

Fig. 2 Initial magnetization curve and corresponding derivative curve (inset) of single-phase permanent $Nd_2Fe_{14}B$ magnet. The pinning field is revealed from the derivative curve

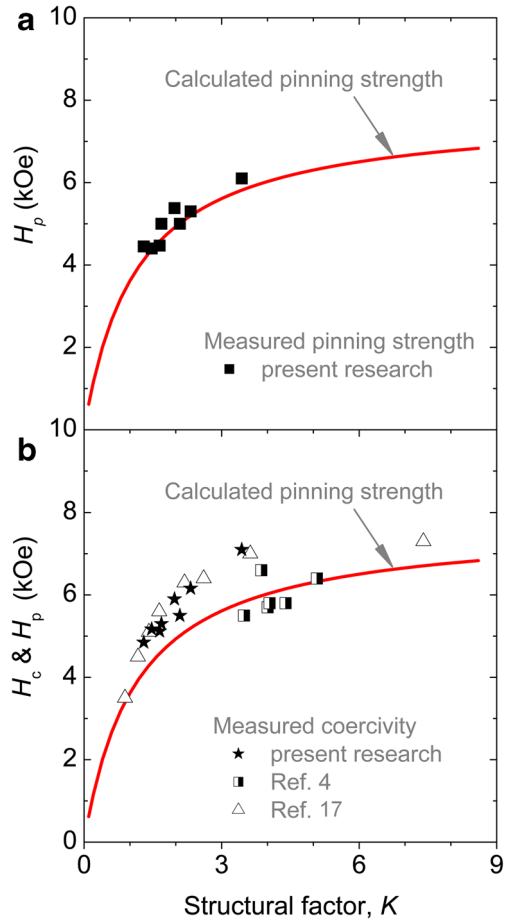

Fig. 3 Dependence of pinning strength (H_p) and coercivity (H_c) of $Nd_2Fe_{14}B/\alpha$-Fe nanocomposite magnet on structural factor (K). The solid squares in **a** and stars in **b** are experimental values in the present research. The half-solid squares and hollow triangles are reported data in refs. [4] and [17]. The red curve in **a** and **b** is the calculated H_p–K curve given by our model

mechanism could be neglected in these samples. Therefore, the coercivity was almost the same as the pinning strength. A high K indicates a high fraction of the hard–hard grain interface with a high grain interface pinning strength, and a low fraction of the hard–soft and soft–soft grain interfaces with a low grain interface pinning strength, thereby leading to a high pinning strength and further a high coercivity. However, the solid star and hollow triangles showed different behaviors. In these samples, the ratio of the calculated pinning strength to the measured coercivity was calculated as $\sim$ 0.9. The difference between the pinning strength and coercivity implies that the coercivity of the samples may be determined by the pinning and nucleation mechanisms together, but the former might be dominant.

To elucidate the coercivity mechanism of the nanocomposite magnets, an important triple-layered mode, i.e., a soft layer with varying thickness sandwiched between two hard layers, was proposed by Zhao's group [18–20]. According to their model, the dominant coercivity mechanism switches from nucleation to pinning as the thickness of the soft interlayer increases from 13 to 30 nm. The model presents the relation between the coercivity and the thickness of soft layer and provides a possibility to predict the coercivity of multi-layered composite magnets. However, for the nanocomposite magnets, pinning is the dominant mechanism due to the existence of numerous grain interfaces [6, 11–13]. Therefore, the grain sizes and phase composition should be considered to predict the pinning strength.

It is well-known that both high coercivity and high remanence are necessary to obtain a large energy product. To achieve a high remanence, a high-volume fraction (up to $\sim$ 50%) and a small grain size ($\sim$ 10 nm) of soft phase are necessary. This conclusion originates from the remanence enhancement induced by the exchange coupling between hard and soft grains as previously reported [21, 22]. Unfortunately, this requirement of high remanence on microstructure conflicts with the requirement of high K. The paradox between the coercivity and the remanence limits the enhancement of energy products for nanocomposite magnets.

To address this issue, new fabrication principles and technologies have been devised to engineer the nanostructures, such as high-pressure (HP) annealing [15], hot deformation (HD) [16], severe plastic deformation (SPD) [23, 24], high-pressure thermal compression (HPTC) [11, 12], and the HPTC coupled with the design of layered structures [13]. These approaches enable the generation of the hard and soft phases with their ideal structures, which open up the opportunities to engineer a bulk nanocomposite with high coercivity [13]. As a result, more recently, breakthrough progress has been realized in achieving record-high energy products in bulk nanocomposite magnets [12, 13], exceeding the values of their corresponding pure rare-earth magnets.

We suggest that the grain-boundary (or interface) pinning strength depends not only on the phase constituent and grain size of the hard and soft nanograins but also on their interfacial structure [24–27]. Therefore, the effect of grain-boundary structures (or interfacial structures) on the pinning strength will be further studied theoretically and experimentally in our work, where the methods of atomic-scale characterization of interfacial structures are highly required such as positron annihilation technology [28].

4 Conclusion

A simple model based on the pinning effect of grain boundaries (interfaces) was proposed to describe the dependence of the pinning strength of nanocomposite magnets

on microstructural parameters. According to the model, a large structural factor K can yield high pinning strength and thus high coercivity in nanocomposite magnets. In particular, refining the grain size of the hard phase was proposed as an effective way to enhance the pinning strength of nanocomposite magnets.

Acknowledgments We thank Mrs. H.L. Li and B. Li for their assistance in the preparation of samples and helpful discussions.

Funding Information The authors gratefully acknowledge the financial support from the National Natural Science Foundation of China (Nos. 51471144, 51471145, 51771163, and 51421091) and the Science and Technology Research Project of Hebei Province (No. ZD2016076).

References

1. Herzer, G.: IEEE Trans. Magn. **26**, 1397 (1990)
2. Manaf, A., Buckley, R.A., Davies, H.A., Leonowicz, M.: J. Magn. Magn. Mater. **101**, 360 (1991)
3. Yin, M., Hu, J., Liu, Y., Wang, Z.X., Lin, W.G.: Chin. Phys. Lett. **7**, 330 (1990)
4. Billoni, O.V., Urreta, S.E., Fabietti, L.M., Bertorello, H.R.: J. Magn. Magn. Mater. **187**, 371 (1998)
5. Sun, X.K., Zhang, J., Chu, Y.L.: Appl. Phys. Lett. **74**, 1740 (1999)
6. Zhao, G.P., Wang, X.L., Yang, C., Xie, L.H., Zhou, G.: J. Appl. Phys. **101**, 09K102 (2007)
7. Feng, W.C., Gao, R.W., Yan, S.S., Li, W., Zhu, M.G.: J. Appl. Phys. **98**, 044305 (2005)
8. Li, Z.B., Shen, B.G., Niu, E., Sun, J.R.: Appl. Phys. Lett. **103**, 062405 (2013)
9. Fischer, R., Schrefl, T., Kronmüller, H., Fidler, J.: J. Magn. Magn. Mater. **153**, 35 (1996)
10. Skomski, R., Coey, J.M.D.: Phys. Rev. B **48**, 15812 (1993)
11. Li, X.H., Lou, L., Song, W.P., Zhang, Q., Huang, G.W., Hua, Y.X., Zhang, H.T., Xiao, J.W., Wen, B., Zhang, X.Y.: Nano Lett. **17**, 2985 (2017)
12. Li, X.H., Lou, L., Song, W.P., Huang, G.W., Hou, F.C., Zhang, Q., Zhang, H.T., Xiao, J.W., Wen, B., Zhang, X.Y.: Adv. Mater. **29**, 1606430 (2017)
13. Huang, G.W., Li, X.H., Lou, L., Hua, Y.X., Zhu, G.J., Li, M., Zhang, H.T., Xiao, J.W., Wen, B., Yue, M., Zhang, X.Y.: Small **14**, 1800619 (2018)
14. Friedberg, R., Paul, D.I.: Phys. Rev. Lett. **34**, 1234 (1975)
15. Zhang, X.Y., Zhang, F.X., Zhang, J.W., Yu, W., Zhang, M., Zhao, J.H., Liu, R.P., Xu, Y.F., Wang, W.K.: J. Appl. Phys. **84**, 1918 (1998)
16. Liu, Y.G., Xu, L., Wang, Q.F., Li, W., Zhang, X.Y.: Appl. Phys. Lett. **94**, 172502 (2009)
17. Bauer, J., Seeger, M., Zern, A., Kronmüller, H.: J. Appl. Phys. **80**, 1667 (1996)
18. Zhao, G.P., Wang, X.L.: Phys. Rev. B **74**, 012409 (2006)
19. Zhao, G.P., Zhao, M.G., Lim, H.S., Feng, Y.P., Ong, C.K.: Appl. Phys. Lett. **87**, 162513 (2005)
20. Si, W.J., Zhao, G.P., Ran, N., Peng, Y., Morvan, F.J., Wan, X.L.: Sci. Rep. **5**, 16212 (2015)
21. Coehoorn, R., Mooji, D.B., DeWaard, C.: J. Magn. Magn. Mater. **80**, 101 (1989)
22. Kneller, E.F., Hawig, R.: IEEE Trans. Magn. **27**, 3588 (1991)
23. Li, W., Li, L.L., Nan, Y., Li, X.H., Zhang, X.Y., Gunderov, D.V., Stolyarov, V.V., Popov, A.G.: Appl. Phys. Lett. **91**, 062509 (2007)
24. Li, H.L., Lou, L., Hou, F.C., Guo, D.F., Li, W., Li, X.H., Gunderov, D.V., Sato, K., Zhang, X.Y.: Appl. Phys. Lett. **103**, 142406 (2013)
25. Sepehri-Amin, H., Ohkubo, T., Hono, K.: Acta Mater. **61**, 1982 (2013)
26. Balamurugan, B., Sellmyer, D.J., Hadjipanayisc, G.C., Skomski R.: Scr. Mater. **67**, 542 (2012)
27. Zhang, X.Y., Guan, Y., Zhang, J.W.: Appl. Phys. Lett. **80**, 1966 (2002)
28. Zhang, X.Y., Sprengel, W., Staab, T.E.M., Inui, H., Schaefer, H.-E.: Phys. Rev. Lett. **92**, 155502 (2004)